University of St Andrews
School of Medicine

The Lipidome: A Case Study of Treatment-Resistance in Clear Cell Renal Cell Carcinoma using Patient Derived Organoids

Submitted as a 2026 Summer Research Project as part of the Laidlaw Scholars Programme

Laidlaw Scholar:
Sultan Chatila

Supervised by:
Prof. David Harrison

LAIDLAW SCHOLARS

Introduction

Renal Cell Carcinoma (RCC) is the sixth most common cancer in the United Kingdom, accounting for ~14,537 cases and 5200 deaths annually. Clear cell renal cell carcinoma (ccRCC), RCC's predominant subtype, is responsible for over 75% of the aforementioned cases. Outcomes are variable, with the mean ten year survival being estimated at 55.6% (1). Its aetiology primarily lies in an inactivation mutation of the VHL gene (3p25), which facilitates unregulated cellular proliferation (2).

Morphologically, ccRCC is characterized by a clear cytoplasm with high intratumoral heterogeneity; both being driven by metabolic reprogramming and lipid accumulation (3). Lipids play a well-established role in ccRCC progression. Increased lipid abundance is known to favour tumorigenesis and contribute to pro-oncogenic adaptations that support cancer cell survival and treatment resistance (4,5,6). Increasing understanding of the lipidome can allow us to identify various metabolic targets for treatment while also enhancing the current treatments available to patients.

Patient derived organoids [tumoroids] (PDOs) have emerged as novel methods to investigate cancer pathology and treatment. The standard 2D cell-based arrays are simple, yet, they fail to accurately capture the structural complexity and pathophysiology of in vivo tissue (7). PDOs have been shown to accurately retain and recapitulate histopathological characteristics, allowing the models to faithfully replicate patients' unique biology. (8).

Mass Spectrometry (MS) is the standard and most commonly used method to investigate lipids (9). MS works by ionizing sample molecules, sorting them by their mass-to-charge ratio (m/z), and measuring their abundance (10). In this investigation, desorption electrospray ionization mass spectrometry imaging (DESI-MSI) was employed. In DESI, an electrospray of solvent droplets impacts the sample surface, gently lifting the target molecules off the surface of the sample. This maintains the tissue, facilitating continual and repeated analysis (11). DESI-MSI utilizes two modes, depending on how analytes are ionized. Positive mode protonates $(M + H^+)$ analytes, while negative mode deprotonates $(M - H^+)$ analytes (12). Both modes were used, which allowed a wider profile of lipids to be generated.

NUC-7738, a phosphoramidate derivative of cordycepin, has been shown to overcome cancer resistance mechanisms in vitro and vivo. Upon conversion into its active metabolite, 3'dATP, it works to disrupt polyadenylation of RNA and key enzymes including RUVBL2, Proteasomes and AAA Atpases. Thus, NUC-7738 is able to increase cancer cell stress and favour synthetic lethality (13, 14). Despite increasing evidence that lipid metabolism contributes to therapeutic response in ccRCC, little is known about how NUC-7738 or immune checkpoint inhibition can remodel the spatial lipidome. This study aims to uncover the effects of NUC-7738 and two immune checkpoint inhibitors, Nivolumab and Ipilimumab on the lipidome of ccRCC, with the goal of identifying lipid species associated with treatment resistance or susceptibility.

Results

Patient Derived Tumoroids Recapitulate Histological and Morphological Characteristics of Original Tissue

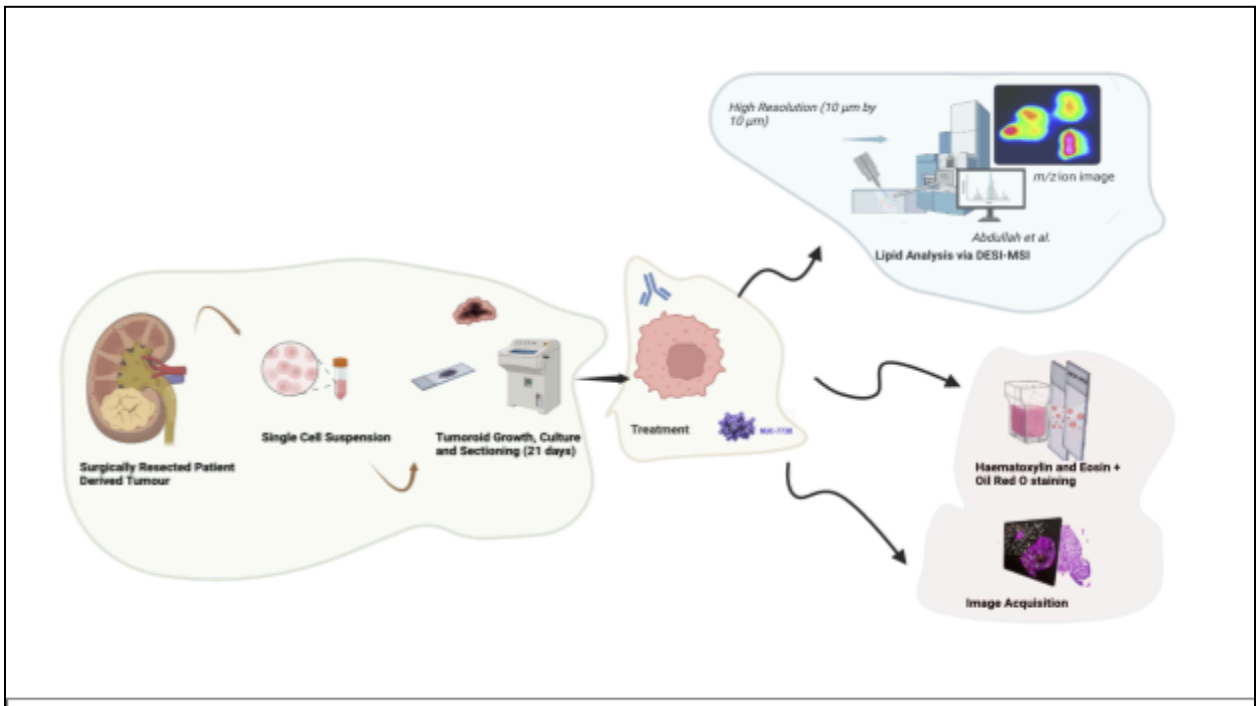

Fig. 1: Diagram Outlining the Harvesting, Preparation, Treatment and subsequent analysis of ccRCC tumoroids

Tumoroids (N=1) were established from freshly dissociated renal tumour tissue by mechanically mincing specimens, followed by enzymatic digestion in Advanced DMEM/F12 containing 5 mg/mL Collagenase Type II and 10 µM Y-27632 ROCK inhibitor. Cells were subsequently cultured in Medium comprising Advanced DMEM/F12 supplemented with 10% fetal calf serum (FCS), 50 ng/mL human epidermal growth factor (hEGF), GlutaMAX, HEPES, and penicillin/streptomycin/amphotericin B. Tumoroids were cultured for approximately 21 days before downstream experimentation (Figure 1). Following growth, tumoroids were stained with Haematoxylin and Eosin (H and E) and Oil Red O (ORO). H and E staining showed a compact nested growth pattern, clear cytoplasmic vacuoles, mirroring the cellular architecture of the primary tissue (Figure 2a, 2b). ORO confirmed the presence of neutral lipid retention and triglycerides within the cells (Figure 2b). Finally, immunofluorescence was used to mark PDL1, CTLA4, CD45 receptors highlighting the presence of an immune cell population within the tumour (Figure 3).

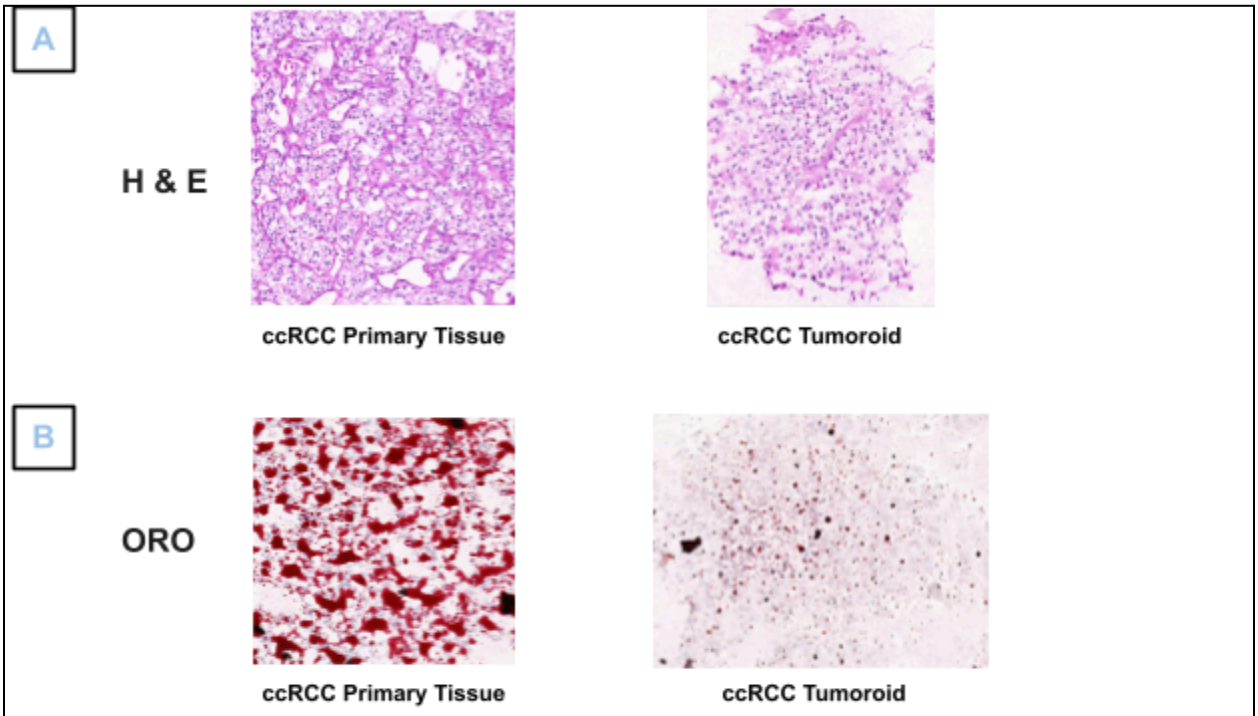

Figs. 2a and 2b: Histological characterisation of ccRCC PDOs

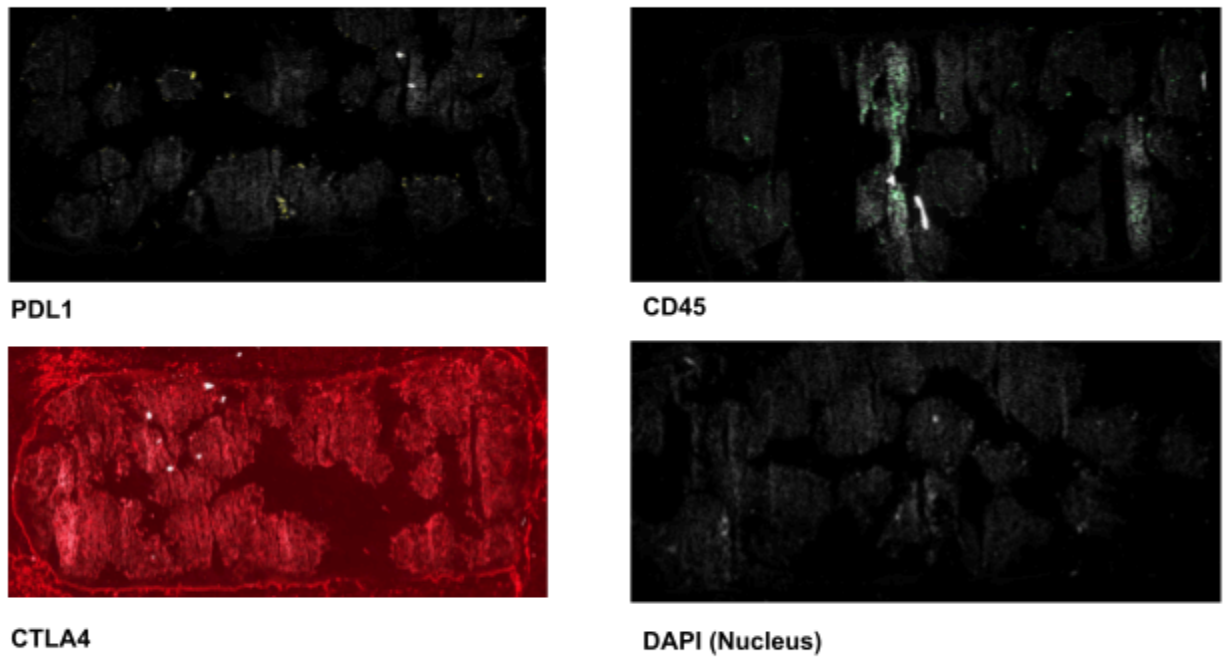

Fig. 3: mIF panels highlighting immune population within tumoroids following treatment

Therapeutic treatment induces a time-dependent increase in apoptosis in ccRCC tumoroids

Over a period of 2 and 5 days, samples were treated with Nivolumab (5ug/ml), Ipilimumab (5ug/ml), NUC - 7738 (10uM), Nivolumab + Ipilimumab, NUC-7738 + Nivolumab and a combination of all three drugs (Figure 4). DMSO served as a negative control while stimulated immune cells were used as a positive control. Each sample was tagged with Annexin V to mark apoptosis across a period of 150 hours. At 48 hours, apoptosis ranged from ~9% (7738 + Nivolumab) to ~35% (NUC-7738). By 120 hours, apoptosis increased in all treatment groups. Between groups, NUC-7738 was responsible for causing the highest level of apoptosis (~46%), while Nivolumab caused the lowest (~13%). The effects of Nivolumab increased marginally when combined with NUC 7738 and Ipilimumab (Figure 5). The observed differences in apoptotic response enabled subsequent stratification of treatment groups into high-apoptosis (NUC-7738, ipilimumab, stimulated immune cells and combination) and low-apoptosis (nivolumab, nivolumab + ipilimumab, and NUC-7738 + nivolumab) categories for lipidomic analyses.

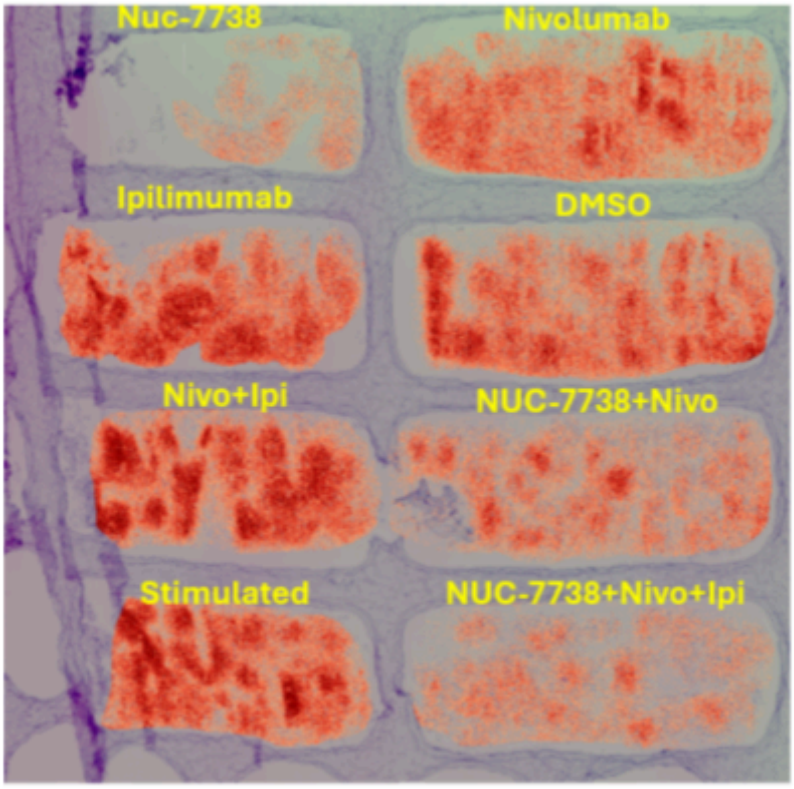

Fig. 4: Conditions Applied to ccRCC Tumoroids

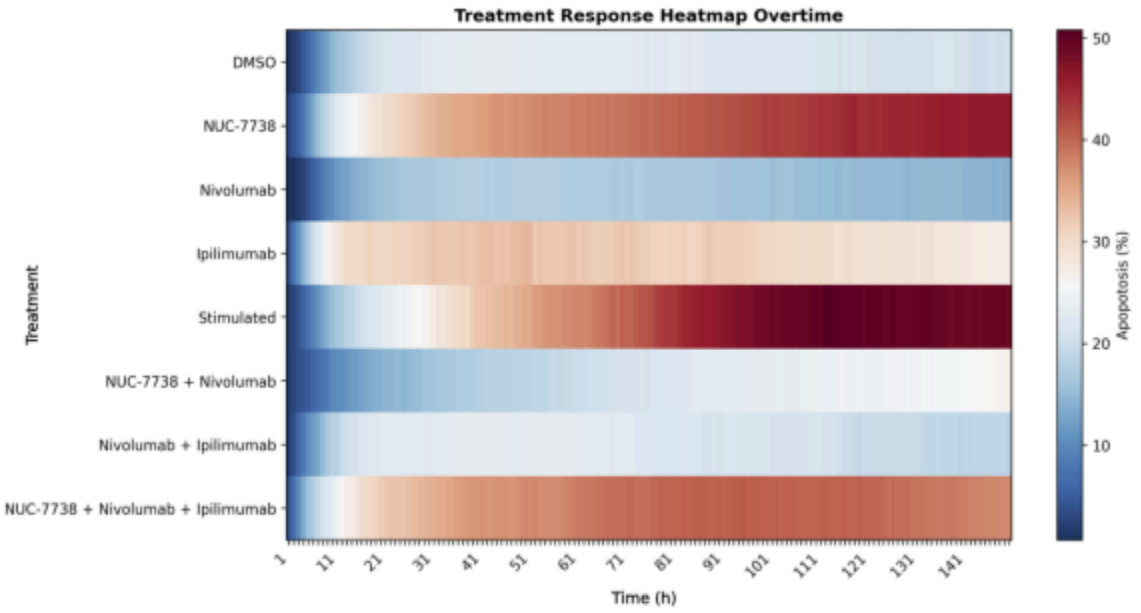

Fig. 5: Heatmap Depicting Apoptosis of Tumoroids Overtime

High-resolution DESI-MSI enables spatial profiling of lipid signatures in ccRCC tumoroids

A renal cell carcinoma cell line was used to optimize the DESI-MSI machine based on signal intensity and the resolution of each individual cell. Following optimization, tumoroids were analysed by DESI-MSI at a 10 x 10 µm pixels in negative and positive mode, yielding single cell resolution. Processing identified 500 raw peaks, between 90-1090 M/Z. By comparing the heatmap of lipids to the structure of the tumoroids within the H and E, background peaks were filtered out, producing peaks that were only present on tissue. This yielded N=299 (Day 2) and N=313 (Day 5) peaks in negative mode and N=168 (Day 2) and N=209 (Day 5) peaks in positive mode (Figure 6a). 59 Regions of interest (ROIs) were then selected to capture the filtered peaks across all 8 conditions. Edges were avoided to prevent the presence of spectral artefacts within the sample (Figure 6b). ROIs were exported in an MVA file and uploaded to Metaboanalyst 6.0 for further processing.

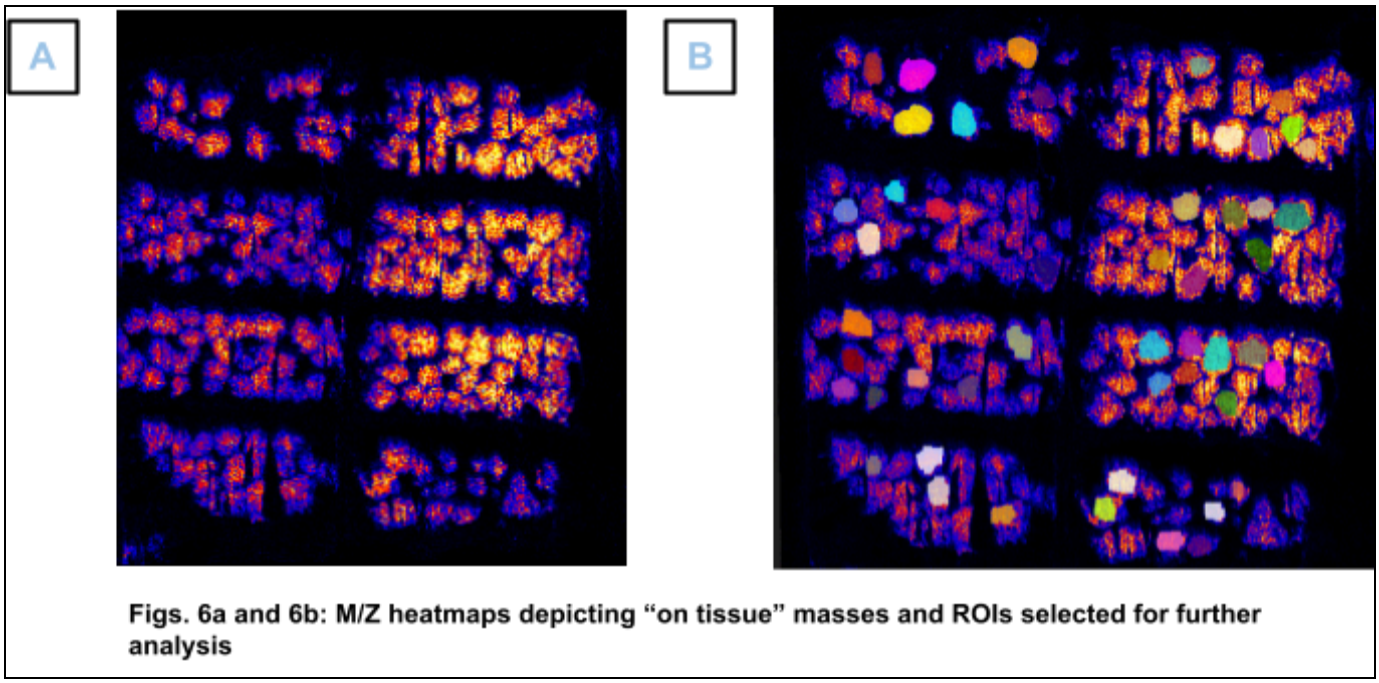

Figs. 6a and 6b: M/Z heatmaps depicting "on tissue" masses and ROIs selected for further analysis

Treatment induces distinct, apoptosis-associated lipidomic signatures in ccRCC tumoroids

Utilizing Metaboanalyst, M/Z figures were normalized using pareto scaling. Principal component analysis (PCA) was performed on normalized lipid abundance data to assess sample clustering and identify patterns of variation between treatment groups in negative and positive mode for Day 2 and Day 5.

Within the day 2 samples, PCA yielded statistically significant differences between Nivolumab (P=0.025), Nivolumab + Ipilimumab (P=0.001) and Stimulated Immune Cells (P=0.005) compared to control (Figure 7). Significance Analysis of Microarrays (SAM) was used to identify differences in specific m/z values across treatment groups. A false discovery rate (FDR) of 0.001 was imposed, as recommended by King et. al (15). SAM identified M/Z values were ranked based on their D values and uploaded to LipidMaps.org and the Human Metabolome Database to determine corresponding lipid species. Larger absolute d-values indicate stronger discriminatory power between treatment groups. SAM identified statistically significant lipid presences were present in the latter two groups. Various Phosphatidyl species (eg. Phosphatidylethanolamine (PE) O-38:6 [D = +6.01, + 2.26], Phosphatidylserine (PS) 36:1 [D = +6.37, +2.57], and Phosphatidylglycerol (PG) 40:7 [D = +5.41, + 2.81]) were enriched in the Nivolumab + Ipilimumab and Stimulated Immune Cells groups. Additionally, both groups saw a lower abundance of fatty acid species (eg. FA 18:1; O2 [D=-6.77, -4.17], FA 16:1; O [D=-5.98 -3.48]).

PCA performed on Day 5 samples revealed distinct treatment specific clustering between all treatments compared with control (P=0.001), highlighting lipidomic heterogeneity across the subgroups (Figure 8). SAM yielded statistically significant differences in lipid presence in all groups, except combination. Treatment groups in the high apoptosis group generally showed an increase in fatty acid abundance (eg. NUC-7738 - Fatty Acid 18:1;O [D = +5.5123], Ipilimumab - Fatty Acid 20:1;0 [D=+2.8075]). Specifically, Fatty Acid 18:1;O had the strongest association with apoptosis. A Pearson's correlation reported R = 0.78 when comparing Fatty Acid 18:1;O abundance (as given by the D value) with the percent apoptosis in each treatment. The high apoptosis groups also saw an overall decrease in triglyceride (TG) abundance (eg. Ipilimumab - Triglyceride 57:7 [D= - 4.82]). This pattern was present in numerous types of TG species including, short-chain, long chain, saturated, mono- and polyunsaturated. For example, TG 15:0/20:4 was repeatedly depleted across all high apoptosis groups (NUC-7738 [D = -3.95], Ipilimumab [D = -2.19], Stimulated Immune Cells [D=-2.56]). Notably, Gangliosides (eg. GM1 [D=-3.41]) and Phosphatidyl Species (eg. Phosphatidylethanolamine (PE) 34:1 [D= -3.453],Phosphatidylinositol (PI) O-33:2 [D=-3.7219], Phosphatidylcholine 35:3 [D=-3.56]), were present in lower abundances in the NUC-7738 group, a pattern not seen in other treatments.

Next, each lipid signature was indexed and displayed on a heatmap generated from DESI-MSI imagining using HDI software. Fatty acids 18:1;O, 18:2;O and 20:1;O were more concentrated in the center of tumoroids in all Day 5 high apoptosis groups. These fatty acid rich areas generally corresponded to areas of necrosis within the H and E stains (Figure 9). Contrastingly, the distribution of TG signatures were not localized to a specific area within tumoroids. Rather they were present in the center, edges or uniformly spread out across the entire tumoroid (Figure 10). Thus TG species corresponded with regions of both necrosis and survival when compared to H and E.

Treatment groups within the low-apoptosis category demonstrated a different lipidomic profile, though patterns were less clear. For example, Nivolumab showed an increased abundance of various Phosphatidyl species (Eg. PI 38:4 [D=3.85], PE[D=3.67). This was contrasted by the Nivolumab + Ipilimumab which exhibited lower Phosphatidyl species (eg. PE 34:0 [D= -3.95], Phosphatidic Acid [D= -3.76]) and mitochondrial associated Cardiolipin (CL) Species (eg. CL 70:0 [D=-3.90], CL 74:0 [D = - 3.76]). Fatty acid signatures were not present in the SAM analysis.

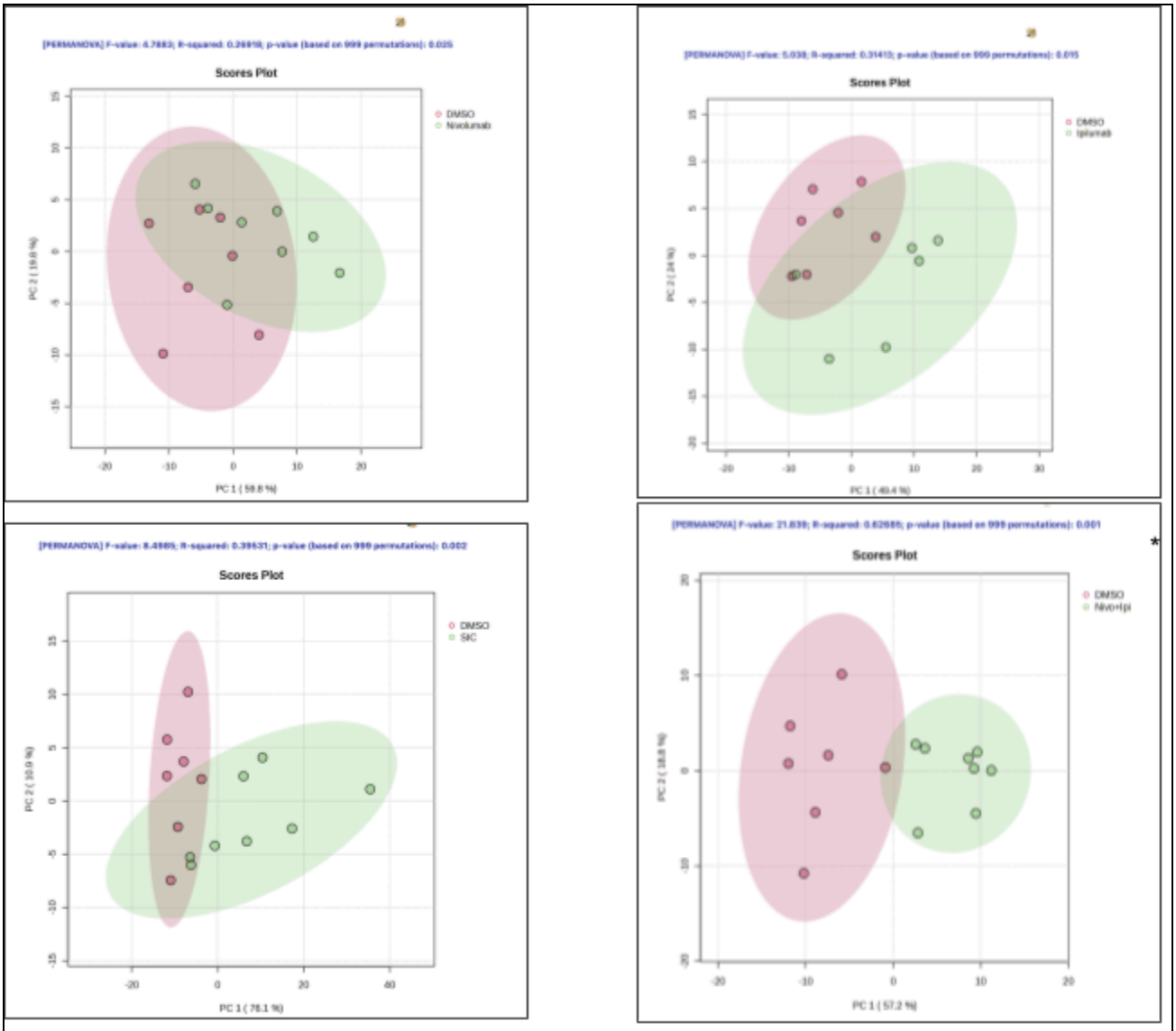

Fig. 7: PCA analysis performed on Day 2 NEG m/z values

**Nivo + Ipi = Nivolumab + Ipilimumab, SIC = Stimulated Immune Cells*

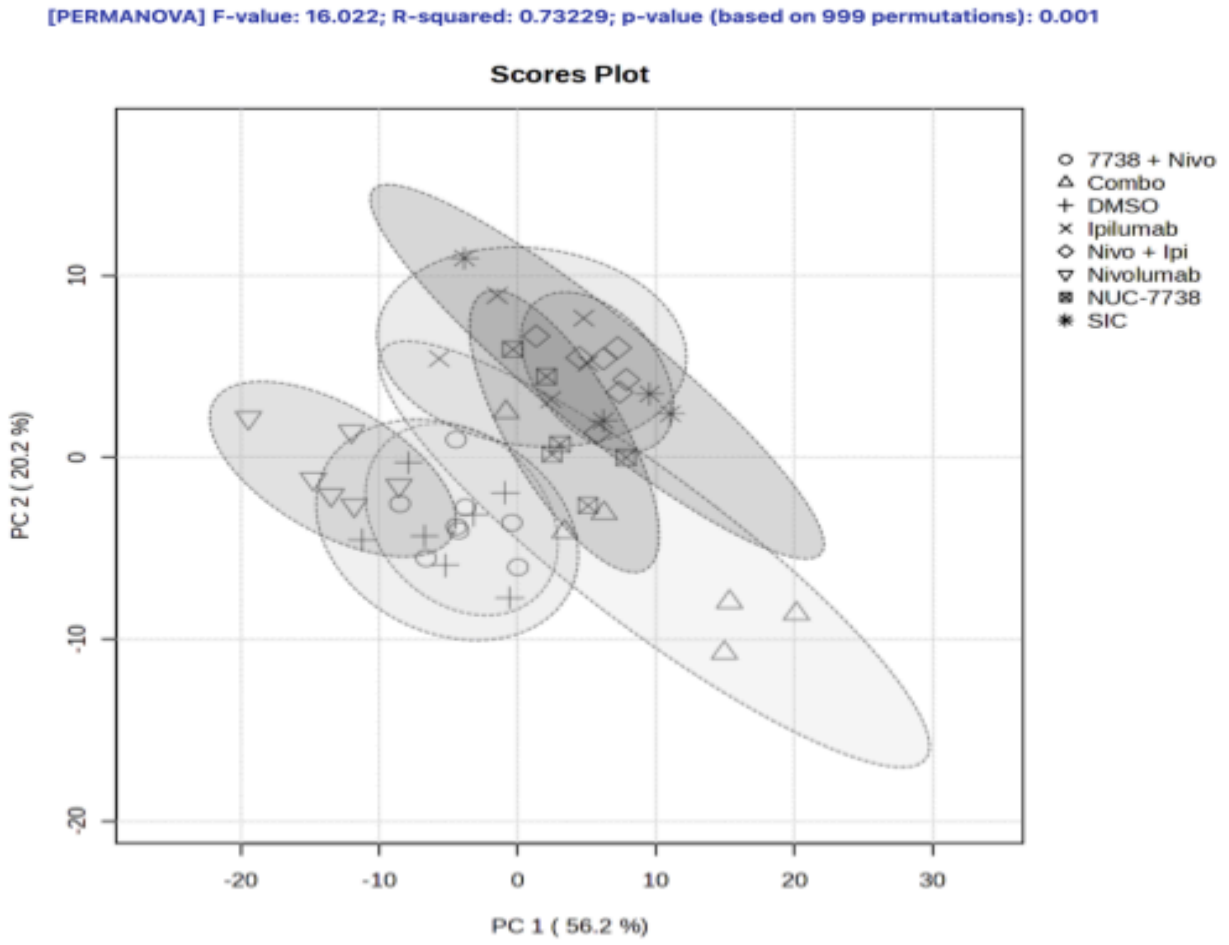

Fig 8. PCA analysis performed on Day 5 NEG m/z values

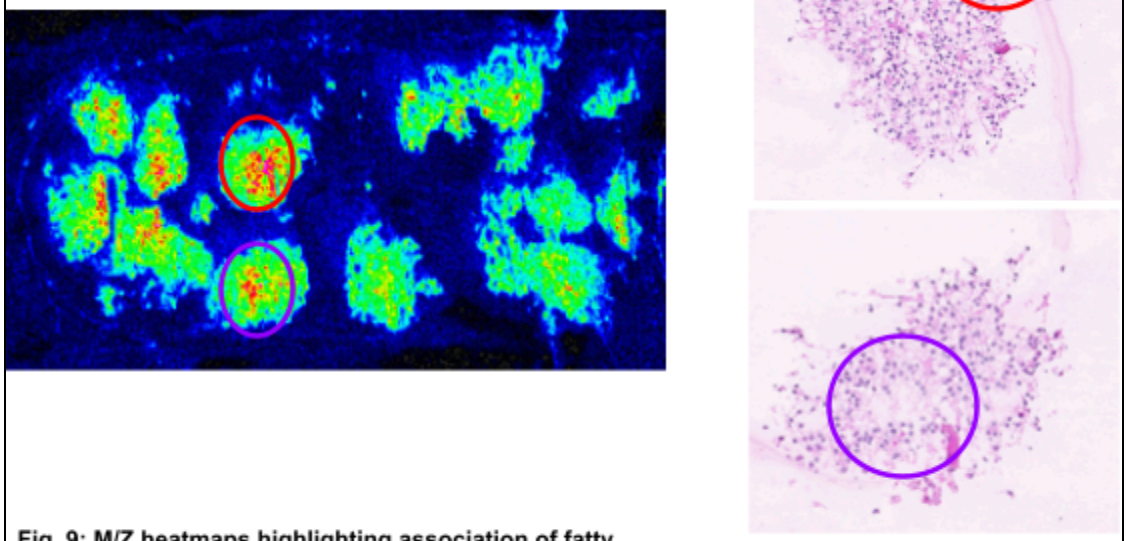

Fig. 9: M/Z heatmaps highlighting association of fatty acids with areas of necrosis on the H and E stain

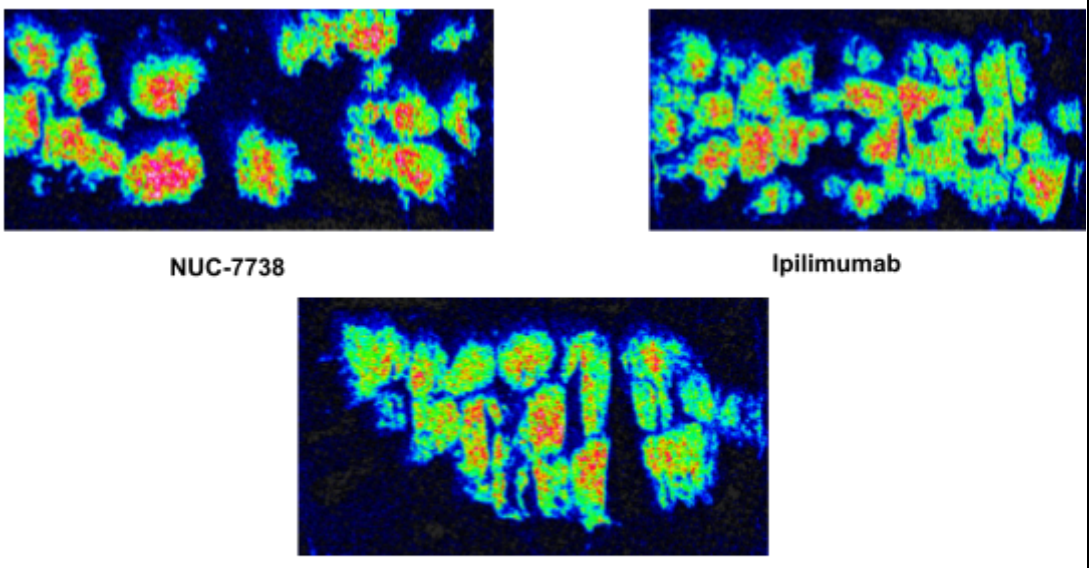

Fig. 10: M/Z heatmaps highlighting uniform distribution of TG 15:0/20:4 (M/Z - 925.7092)

The same process was repeated in positive mode. Day 2 PCA yielded statistically significant differences in NUC-7738 (P=0.001), Nivolumab + Ipilimumab (P=0.001) and Stimulated Immune Cells (P=0.002) (Figure 11). SAM yielded significant metabolites in all groups. NUC-7738 showed an increase in two metabolites: PC O-35:1 [D=2.11] and TG 15:O/20:2/O-18:O (D=2.08). 16 TG species were decreased in Nivolumab + Ipilimumab (eg. TG 56:1 [D=-1.76]). Similarly to negative mode, this group saw a lower quantity of phosphatidyl species (eg. PC 46:0 [D=-1.79], PE 24:0 [D=-1.80]) and Diacylglycerol [D=-2.96]. Finally, stimulated immune cells showed a decrease in various TG species (eg. TG 54:0 [D=-2.91]) and an increase in PC species (eg. PC 38:5 [D=2.11], PC O-37:1 [D=3.49]). Again, PCA performed on Day 5 samples revealed distinct treatment specific clustering between treatments compared with control (P=0.001) (Figure 12). However, lipidomic patterns were less clearly associated with apoptotic response and instead segregated according to the presence or absence of immune checkpoint inhibitors. Ipilumumab, Ipilumumab + Nivolumab and Nivolumab all showed an increased abundance of PG, PS, PE, PA species. For example, PS 37:2 was elevated in all the aforementioned groups [D = +6.82, ,+2.35,+ 3.63 respectively]. Additionally, Ipilumumab, Ipilumumab + Nivolumab and combination shared a lowered abundance of oxidized lysophospholipid LPC O-10:1 [D = -4.72, -3.62, -6.96 respectively]. Conversely, LPC O-18:2 was upregulated in Ipilumumab [D=+6.48] and Ipilumumab + Nivolumab [D=+2.35]. Comparison of the identified lipid signatures with hIF images containing immune cells did not reveal clear spatial correspondence between specific lipids and individual immune cell populations, with several lipid signals instead overlapping with regions identified as background. TG species were present in both increased and decreased quantities across all groups. NUC-7738's profile was characterised by a reduction in both oxidized and non oxidized triglyceride species (eg. TG(15:0/O-18:0/20:3) [D = -3.54] alongside an increased abundance of sphingomyelin (SM) species (eg. SM18:2/23:1 [D = 1.70]). The latter was also observed following Ipilimumab and Nivolumab treatment. SAM yielded no significant metabolites for NUC-7738 + Nivolumab.

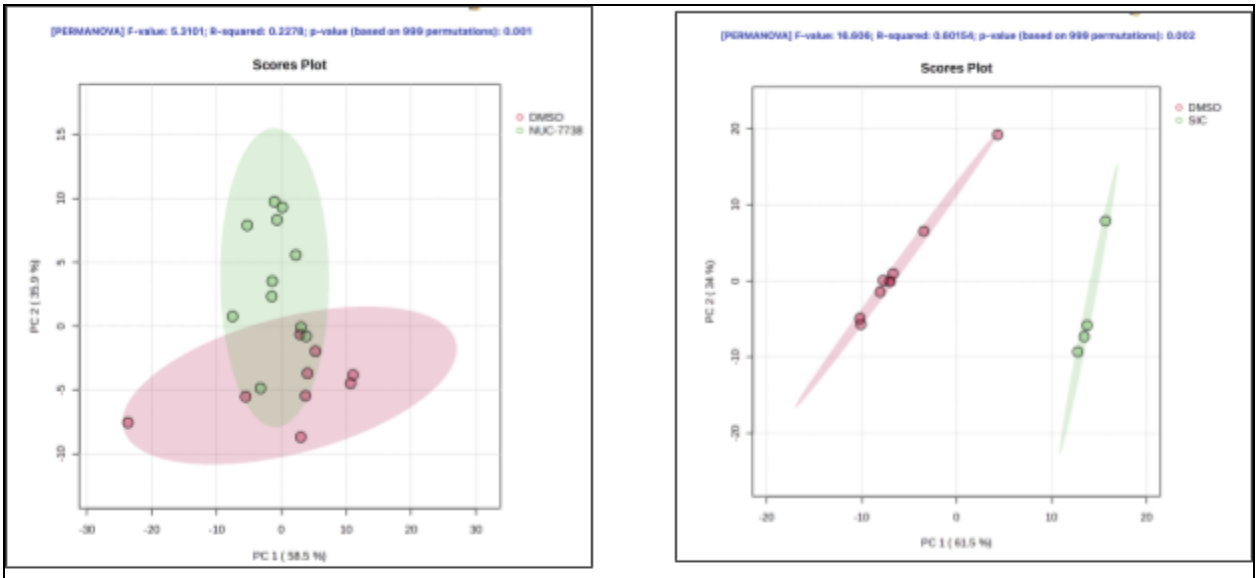

Fig. 11: PCA analysis performed on Day 2 POS m/z values

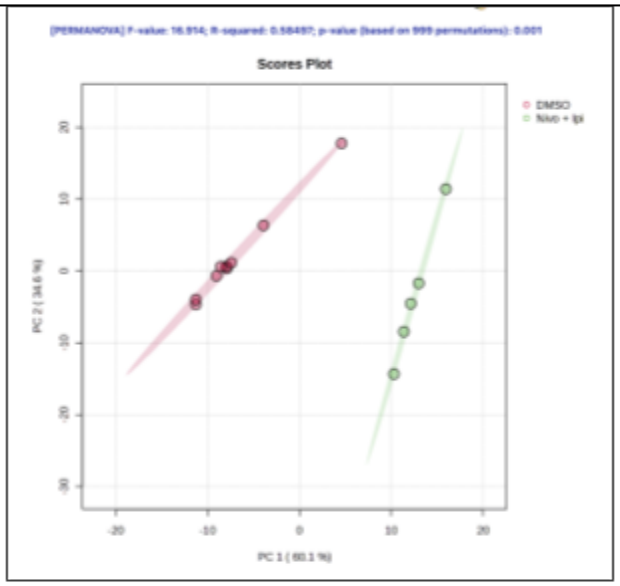

Fig. 11 cont'd: PCA analysis performed on Day 2 POS m/z values

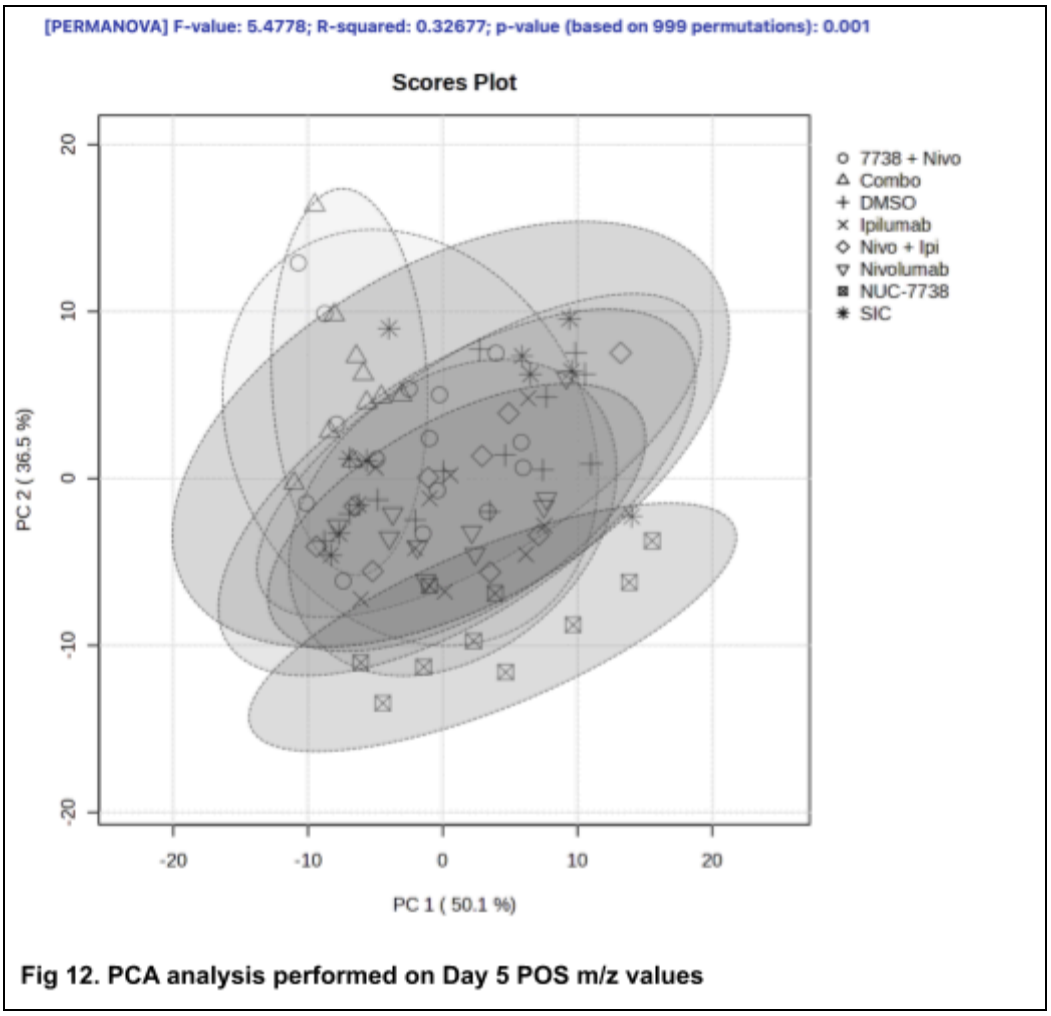

Fig 12. PCA analysis performed on Day 5 POS m/z values

Discussion

The findings of this study suggest that NUC-7738 and immune checkpoint inhibitors Nivolumab and Ipilimumab change the lipidome as part of their function. Subsequent analysis revealed lipid signatures that may be associated with necrosis, normal and dysregulated metabolism.

As revealed by SAM, mono and poly -unsaturated oxidized fatty acids, such as FA 18:1; O and FA 18:2; O, clustered within treatment groups that caused higher apoptosis. Oxidized fatty acid species have been shown to function as bioactive lipid mediators that promote apoptosis in cancer cells by activating mitochondrial apoptotic pathways, increasing ROS production, and inducing caspase-dependent cell death (16). Further, fatty acid presence was shown to be localized to the center of the tumoroid, which are commonly necrotic (17). Finally, the correspondence of target M/Z to areas of necrosis on the H and E stain supports the potential use of fatty acids as a marker of cell death.

Li *et a*l. demonstrated that saturated, monounsaturated, and polyunsaturated TG species can influence cancer progression across multiple malignancies, including hepatocellular carcinoma (18). In the present study, all TG species were decreased within the high-apoptosis treatment groups, with NUC-7738 producing the greatest reduction relative to DMSO. This reduction may reflect disruption of lipid storage and metabolic processes associated with tumour viability. Furthermore, Muz *et al.* highlighted the presence of metastatic activity within both the invasive tumour edge and hypoxic tumour core (19). TG species identified in the present study were detected across both the centre and edge of the tumoroids, with relatively uniform spatial distribution. Taken together, these findings suggest that the observed reductions in TG abundance may reflect alterations in lipid metabolic pathways present across spatially distinct tumour regions, which may have implications for both tumour viability and progression.

Phosphatidyl species represent a more multifaceted lipid signature, with established roles in membrane structure, cellular signalling, cancer progression, and immune-cell function. Phosphatidylserine and phosphatidylcholine contribute to the structural and functional properties of cellular membranes and have been implicated in cellular responses to apoptotic and other forms of stress. In cancer, altered phosphatidylserine signalling has also been associated with tumour immune suppression and disease progression (20). Conversely, phosphatidyl species undergo substantial remodelling during immune-cell activation. In proliferating T cells, stimulation has been shown to alter the distribution of phosphatidylcholine, phosphatidylinositol, and phosphatidylethanolamine, including increased abundance of specific PE species (21).

The increased abundance of PG, PS, PE, and PA species observed in the Nivolumab, Ipilimumab, and Nivolumab + Ipilimumab groups may therefore be consistent with phospholipid remodelling associated with immune activation. However, these patterns were less clearly associated with survival and spatial comparison with hIF immune-cell regions did not reveal consistent correspondence between individual phosphatidyl species and immune-cell populations. Consequently, the observed phosphatidyl changes may reflect a combination of tumour-cell membrane adaptation, treatment-associated stress responses, and immune-cell lipid remodelling. More refined spatial approaches, such as pLSA, would be required to distinguish between these possibilities and determine the cellular origin of the observed phosphatidyl signatures.

NUC-7738 specifically reduced the abundance of the Gangliosides GM1 relative to DMSO, whereas no reduction was observed following the other treatments. GM1 and GM2 have previously been implicated in the regulation of cancer cell migration and invasion across various cell-lines (22) Thus, the selective reduction of these gangliosides following NUC-7738 treatment may indicate an effect on lipid pathways associated with invasive behaviour. This finding warrants further investigation into whether NUC-7738 can modulate tumour invasion and progression in RCC and may provide a basis for evaluating its therapeutic potential in early-stage disease.

An important limitation of this investigation is its sample size. N = 1 limits the generalisability and statistical power of the findings and precludes assessment of inter-sample variability. Future studies should therefore apply this established methodology across larger and diverse sample cohorts to validate the lipid signatures identified in this investigation and determine their reproducibility. Such validation will be essential for establishing whether the

observed lipidomic alterations represent consistent features of treatment response and for further elucidating their potential biological and therapeutic relevance in RCC.

Acknowledgements

I would like to express my deepest gratitude to Lord Laidlaw and the Laidlaw Scholars Foundation for providing me with funds which have enabled me to carry out this project. I would also like to thank my supervisor Prof. David Harrison and his research team, namely Greice Zickuhr for supporting me throughout this process. Thank you for answering all my relentless questions, helping me with the most menial tasks and providing me with an amazing work environment. I am very lucky to have had the opportunity to work with you.

References

1. Cancer Research UK. (2015). Kidney cancer statistics. In *Cancer Research UK*. https://www.cancerresearchuk.org/health-professional/cancer-statistics/statistics-by-cancer-type/kidney-cancer
2. Clear cell. (n.d.). In *www.pathologyoutlines.com*. Retrieved August 9, 2026, from https://www.pathologyoutlines.com/topic/kidneytumormalignantrccclear.html
3. Abdullah, H., Zickuhr, G. M., Um, I. H., Laird, A., Mullen, P., Harrison, D. J., & Dickson, A. L. (2025). Kidney tumoroid characterisation by spatial mass spectrometry with same-section multiplex immunofluorescence uncovers tumour microenvironment lipid signatures associated with aggressive tumour phenotypes. *Npj Imaging*, *3*(1). https://doi.org/10.1038/s44303-025-00106-x
4. Simeth, J., Engelmann, S., Mayr, R., Kaelble, S., Weber, F., Pichler, R., Dettmer, K., Oefner, P. J., Höring, M., Symeou, L., Freitag, K., Wagner, K., Burger, M., Herr, W., Kreutz, M., Spang, R., Liebisch, G., & Siska, P. J. (2025). Lipid metabolism of clear cell

renal cell carcinoma predicts survival and affects intratumoral CD8 T cells. *Translational Oncology*, *61*, 102513. https://doi.org/10.1016/j.tranon.2025.102513

5. Feng, Y., Zhang, S., Li, J., Yue, D., & Wang, Y. (2026). Targeting lipid metabolism to overcome therapeutic resistance in renal cell carcinoma: Mechanisms and emerging strategies. *Current Urology*. https://doi.org/10.1097/cu9.0000000000000355
6. Pearce, S. M., Cross, N. A., Smith, D. P., Clench, M. R., Flint, L. E., Hamm, G., Goodwin, R., Langridge, J. I., Claude, E., & Cole, L. M. (2024). Multimodal Mass Spectrometry Imaging of an Osteosarcoma Multicellular Tumour Spheroid Model to Investigate Drug-Induced Response. *Metabolites*, *14*(6), 315. https://doi.org/10.3390/metabo14060315
7. Liu, X., Weaver, E. M., & Hummon, A. B. (2013). Evaluation of therapeutics in three-dimensional cell culture systems by MALDI imaging mass spectrometry. *Analytical Chemistry*, *85*(13), 6295–6302. https://doi.org/10.1021/ac400519c
8. Abdullah, H., Zickuhr, G. M., Um, I. H., Laird, A., Mullen, P., Harrison, D. J., & Dickson, A. L. (2025). Kidney tumoroid characterisation by spatial mass spectrometry with same-section multiplex immunofluorescence uncovers tumour microenvironment lipid signatures associated with aggressive tumour phenotypes. *Npj Imaging*, *3*(1). https://doi.org/10.1038/s44303-025-00106-x
9. Gerhardtova, I., Timotej Jankech, Majerova, P., Juraj Piestansky, Dominika Olesova, Kovac, A., & Jampilek, J. (2024). Recent analytical methodologies in lipid analysis. *International Journal of Molecular Sciences*, *25*(4), 2249–2249. https://doi.org/10.3390/ijms25042249
10. Mass spectrometry - an overview | ScienceDirect topics. (2015). In *Sciencedirect.com*.

https://www.sciencedirect.com/topics/agricultural-and-biological-sciences/mass-spectrometry

11. Desorption electrospray ionization - an overview | ScienceDirect topics. (n.d.-a). In *www.sciencedirect.com*. Retrieved August 10, 2026, from https://www.sciencedirect.com/topics/biochemistry-genetics-and-molecular-biology/desorption-electrospray-ionization
12. *Spatial metabolomics ion mode selection: Positive vs. negative polarity in MALDI-MSI and DESI-MSI*. (2019). Metwarebio.Com. https://www.metwarebio.com/spatial-metabolomics-ion-mode-selection-positive-vs-negative-polarity-msi/
13. Hagen, S., De Zan, E., Mustafa, E., Ruud, van S., Kudsy, M., Morris, J., Ferrari, V., Um, I. H., Chettle, J., Kazmi, F., Campo, L., Easton, A., Nijman, S., Serpi, M., Symeonides, S., Plummer, R., Harrison, D. J., Bond, G., & Blagden, S. P. (2021). The novel nucleoside analogue ProTide NUC-7738 overcomes cancer resistance mechanisms in vitro and in a first-in-human phase I clinical trial. *Clinical Cancer Research*, *27*(23), 6500–6513. https://doi.org/10.1158/1078-0432.CCR-21-1652
14. NuCana plc. (n.d.-b). In *www.nucana.com*. Retrieved August 10, 2026, from https://www.nucana.com/nuc7738.html
15. King, M. E., Yuan, R., Chen, J., Pradhan, K., Sariol, I., Li, S., Chakraborty, A., Ekpenyong, O., Yearley, J. H., Wong, J. C., Zúñiga, L., Tomazela, D., Beaumont, M., Han, J.-H., & Eberlin, L. S. (2023). Long-chain polyunsaturated lipids associated with responsiveness to anti-PD-1 therapy are colocalized with

immune infiltrates in the tumor microenvironment. *The Journal of Biological Chemistry*, *299*(3), 102902. https://doi.org/10.1016/j.jbc.2023.102902

16. Fatty acids and their lipid mediators in the induction of cellular apoptosis in cancer cells. (2022). *Prostaglandins & Other Lipid Mediators*, *160*, 106637. https://doi.org/10.1016/j.prostaglandins.2022.106637
17. Lotfi, R., & Kaltenmeier, C. (2026). *Until Death Do Us Part: Necrosis and Oxidation Promote the Tumor Microenvironment*. Nih.Gov. https://pmc.ncbi.nlm.nih.gov/articles/PMC4872058/
18. Muz, B., de la Puente, P., Azab, F., & Azab, A. K. (2015). The role of hypoxia in cancer progression, angiogenesis, metastasis, and resistance to therapy. *Hypoxia*, *3*(3), 83. https://doi.org/10.2147/hp.s93413
19. Haberl, E. M., Pohl, R., Rein-Fischboeck, L., Höring, M., Krautbauer, S., Liebisch, G., & Buechler, C. (2021). Accumulation of cholesterol, triglycerides and ceramides in hepatocellular carcinomas of diethylnitrosamine injected mice. *Lipids in Health and Disease*, *20*(1). https://doi.org/10.1186/s12944-021-01567-w
20. Preetam, S., Pandey, A., & Mishra, R. (2024, May 2). *Phosphatidylserine: paving the way for a new era in cancer therapies*. Rsc.Org. https://pubs.rsc.org/ma/article/5/21/8384/853958/Phosphatidylserine-paving-the-way-for-a-new-era-in
21. Tomita, M., Baker, R. C., Ando, S., & Santoro, T. J. (2004). Arachidonoyl-phospholipid remodeling in proliferating murine T cells. *Lipids in Health and Disease*, *3*, 1. https://doi.org/10.1186/1476-511X-3-1

22. Sarkar, A., Banerjee, S., & Biswas, K. (2023). Multi-dimensional role of gangliosides in modulating cancer hallmarks and their prospects in targeted cancer therapy. *Frontiers in Pharmacology*, *14*. https://doi.org/10.3389/fphar.2023.1282572

Appendix

Appendix 1: SAM Results for Day 2 Samples in NEG Mode

7738 vs DMSO

M/Z	Metabolite	D Value
663.4019	PA 34:6 + H+	-4.5244
763.5148		
759.526	PA O-42:7/PG 35:2 + H+	-4.2596
721.4886	PA 38:5 + H+	-4.2142
765.5331	CerPE 38:2;O3 + H+	-4.075
695.559	DG(20:2, 22:4) + H+	-4.0189
777.5554	PA O-40:2 + H+	-3.8598
819.5904	DG **(13M5/13M5/0:0)** / DG(13D5/11D5/0:0) / DG(11D5/13D5/0:0) + H+	-3.6059

Ipilimumab vs DMSO

No Significant Metabolites

Nivolumab + Ipilimumab vs DMSO

M/Z	Metabolite	D Value
750.5398	PE O-38:5	6.7084
788.5426	PS 36:1	6.3716
722.5108	PE O-36:5	6.3314
748.5244	PE O-38:6	6.0883
821.5278	PG 40:6	5.8358
820.5424	PS O-40:6	5.7874
774.5347	PS 35:1	5.6568
700.5251	PE O-34:2	5.4958
819.5165	PG 40:7	5.4123
804.5428	Hex2Cer 30:1;O2	5.3371
822.5311	PS 39:5	5.3212
773.5326	PG 36:2	5.2651

744.5504	CL 74:1	5.2046
789.5406	PA 43:6	4.8672
814.5413	PE 42:8	4.8314
716.5243	PE 34:1	4.7717
751.5455	PA O-38:1	4.7673
802.5407	PE 41:7	4.7671
888.5694	PS 44:7	4.7383
887.5632	PI 38:3	4.6895
812.5317	PE 42:9	4.6695
702.5273		
846.5335		
810.5283	PE O-40:7	4.5456
818.5192	PE 38:4;O	4.5078

786.5253	PS 36:2	4.4951
736.5312		
816.5627	PC O-37:4	4.2969
742.5369	PE 36:2	4.2829
766.5358	PE 38:4	4.214
885.5494	PI 38:4	4.145
844.6277		
790.5411	PE 40:6	4.0569
723.51	PA O-36:1	4.0413
846.6436		
811.5372		
701.5187	CerPE 36:2;O3	4.0161
776.5347	PC O-34:3/PE O-37:3	4.0058

842.6023		
313.2373	FA 18:1;O2	-6.7737
271.2268	FA 16:0;O	-6.0828
269.2113	FA 16:1;O	-5.9842
299.2572	FA 18:0;O	-5.1406
283.227	FA 17:1;O	-4.6099
693.458	PA O-34:2	-4.436
664.4057		
713.3519		
269.2477	FA 17:0	-4.2777
691.4476	PA O-34:3	-4.1055
679.3876	PG 27:2;O2	-4.0684
735.4758	CL 74:10	-4.045

Nivolumab vs DMSO

No significant metabolites

Stimulated vs DMSO

M/Z	Metabolite	D Value
313.2373	FA 18:1;O2	-4.1795
297.2427	FA 18:1;O	-3.6267
269.2113	FA 16:1;O	-3.4845
299.2572	FA 18:0;O	-3.3727
713.3519		
271.2268	FA 16:0;O	-3.0287
283.227	FA 17:1;O/FOH 17:2;O2	-2.9632
695.559		
679.3876	PG 27:2;O2	-2.873
298.2461		
325.2739	FA 20:1;O	-2.6714
663.4019	PA 34:6	-2.614
664.4057		
693.458		
819.5165	PG 40:7	2.821
820.5424	PS O-40:6	2.6598
788.5426	PS 36:1	2.5707
818.5192	PE 38:4;O	2.5534
722.5108	PE O-36:5	2.3109
886.5531	SHexCer 38:1;O3	2.2889
745.5652		

700.5251	PE O-34:2	2.2751
748.5244	PE O-38:6	2.2695
822.5311	PS 39:5	2.2522
887.5632	PI 38:3	2.2512
812.5317	PE 42:9	2.2302
702.5273		
846.5335		
742.5369	PE 36:2	2.1618
814.5413	PE 42:8	2.1533
842.6023		
888.5694	PS 44:7	2.1226
796.518	PS 37:4	2.1219

Combination vs DMSO

No significant metabolites

Appendix 2: SAM Results for Day 5 Samples in NEG Mode

7738 vs DMSO

M/Z	Lipid	D value
297.2421	FA 18:1;O	5.1523
325.2733	FA 20:1;O	4.6596
716.5249	PE 34:1	-3.453
953.7401	TG 57:7 - CL	-4.82
844.6292	PS O-41:1	-3.5308
804.5366	PC 35:3/PE 38:3	-3.5659
805.5256	PI O-33:2	-3.7219
846.6425	PS O-41:0	-3.5744
828.5084	Ganglioside GM1	-3.4108

818.6176	Ceramide-1-Phosphate(d18:1/26:1(17Z))	-3.4808
979.7494	TG(15:0/22:4)	-3.7229
927.723	TG(15:0/18:0/22:6)	-3.82
925.7092	TG(15:0/20:4)	-3.9584
951.7242	TG(15:0/22:4)	-4.2212
954.7441		
926.713		
952.7283		

Nivo vs DMSO

M/Z	Lipid	D value
885.5493	PI 38:4	3.8471
886.5529	SHexCer 38:1;O3/PS 44:8	3.6407
810.5274	PS 38:4	3.6278
742.5374	PE 36:2	3.6007
786.5245	PS 36:2	3.5428
743.547	CL(i-16:0/a-17:0/18:2(9Z,11Z)/23:0) - *PPM = 7*	3.6495

Stimulated vs DMSO

M/Z	Lipid	D value
953.7401	PG O-33:1	-3.2199
718.5436	PE 34:0	-2.2059
717.5294	CL 70:0	-2.181
720.5616	PS O-32:0	-2.1625
297.2421	FA 18:1;O	3.5625
925.7092	TG(15:0/20:4)	-2.5606

951.7242	TG(15:0/22:4)	-2.3308
843.6267	TG(15:0/14:1)	-2.1634
927.723	TG(15:0/18:0/22:6)	-2.6166
691.5252	DG(20:2n6) - PPM = 8	-2.1188
298.2454		
719.5571	CE(20:4) - PPM = 7	-2.9713
956.7546		
926.713		
844.6292		
954.7441		

Nivo + Ipi vs. DMSO

M/Z	Lipid	D value
297.2421	FA 18:1;O	4.666
298.2454		
555.4395		
681.5804	CE(18:1)	3.3945
325.2733	FA 20:1;O	3.3171
718.5436	PE 34:0	-3.965
717.5294	CL 70:0	-3.9092
745.5673	PA 39:0	-3.7685
952.7283	CL 74:0	-3.7607
953.7401	TG(15:0/20:1)	-5.5956
719.5571	CE(20:4) - PPM 7	-4.7851
951.7242	TG(15:0/22:4)	-4.3841
927.723	TG(15:0/18:0/22:6)	-4.0407
843.6267	TG(15:0/14:1/20:5)	-3.7767

331.1895	PA(PGF1alpha/10:0)	-3.6355
720.5616	DG(18:4n3/0:0/18:4n3)	-3.6191
925.7092	TG(15:0/20:4)	-4.3675

Ipilimumab vs DMSO

M/Z	Lipid	Delta
297.2421	FA 18:1;O	4.2371
295.2263	FA 18:2;O	2.8431
325.2733	FA 20:1;O	2.8075
953.7401	TG 57:7 - CL	-2.7914
951.7242	TG(15:0/22:4)	-2.1716
719.5571	CE(20:4) - PPM = 7	-2.4934
925.7092	TG(15:0/20:4)	-2.1891
927.723	TG(15:0/18:0/22:6)	-2.2321
298.2454		
954.7441		

Control Vs DMSO

No significant metabolites

Appendix 3: SAM Results for Day 5 Samples in POS Mode

NUC-7738 vs DMSO

M/Z	Lipid	Delta
429.2559		
766.6001	PG O-35:1 + NH4	2.1109
923.7817		

897.7649	TG(15:0/20:2n6/O-18:0) + K+	2.08
881.7825		

Nivolumab vs DMSO

No significant metabolites

Nivolumab + Ipilumumab vs DMSO

M/Z	Lipid	Delta
693.5467	DG 40:5	-2.9649
881.7825		
907.8006		
909.8149		
882.7889	TG(14:1(9Z)/22:5(4Z,7Z,10Z,13Z,16Z)/O-18:0) + NH4	-2.5354
691.5197		
855.7676		
879.7693		
931.8021		
799.6832	TG 46:1	-2.2889
908.8074	TG(16:1(9Z)/22:6(4Z,7Z,10Z,13Z,16Z,19Z)/O-18:0) + NH4	-2.2632
905.7888	TG(15:0/22:4(7Z,10Z,13Z,16Z)/O-18:0) + Na	-2.1643
929.788	TG 54:0	-2.104
933.8159		
963.842	TG 58:3	-2.074
880.7742	TG(14:1(9Z)/22:6(4Z,7Z,10Z,13Z,16Z,19Z)/O-18:0) + NH4	-2.0631
935.8297		
853.7538		
955.8048	TG 56:1	-2.0069

932.8087	TG(18:3(6Z,9Z,12Z)/22:6(4Z,7Z,10Z,13Z,16Z,19Z)/O-18:0) + NH4	-2.0014
883.8054	TG(15:0/20:1(11Z)/O-18:0) + Na	-1.9816
957.8185	TG 56:0	-1.9757
910.8215	TG(16:0/O-18:0/22:6(4Z,7Z,10Z,13Z,16Z,19Z)) + NH4	-1.9664
856.7731	TG(14:1(9Z)/20:4(5Z,8Z,11Z,14Z)/O-18:0) + NH4	-1.966
643.5439	CE(16:2) + NA	-1.9559
964.8472		
965.8553	TG 58:2	-1.9227
959.8311		
911.82		
673.6132		
876.831		
961.8314	PE-NMe2(24:0/24:0) + NH4	-1.7987
930.7961	PC 46:0	-1.7953
615.5173		
906.7971		
903.7783	TG(15:0/22:5(4Z,7Z,10Z,13Z,16Z)/O-18:0) + Na	-1.7694
939.8322	TG 56:1	-1.7619
850.8148		
854.7585	TG(14:1(9Z)/20:5(5Z,8Z,11Z,14Z,17Z)/O-18:0) + NH4	-1.7442

Ipilimumab vs DMSO

No significant metabolites

NUC-7738 + Nivolumab vs DMSO

M/Z	Lipid	Delta
808.5929	PC 38:5/PE 41:5/PA 43:6 + H	2.1199
810.6276	PC O-37:1 + Na	3.4954

881.7825	PA 35:0 (+H)/DG 40:6 (+Na)	-3.6022
691.5197	DG 40:5 + Na	-3.4201
643.5439	CE(16:2) + Na+	-3.3942
907.8006		
693.5467	DG(20:2n6/0:0/22:6n3) + H	-3.2691
879.7693		
615.5173		
799.6832	TG 46:1 + Na	-3.1559
882.7889	TG(14:1(9Z)/22:5(4Z,7Z,10Z,13Z,16Z)/O-18:0) + NH4	-3.1259
659.5287	HexCer 30:2;O2 + NH4	-3.0728
766.6001	PG O-35:1 + NH4	3.0644
876.831		
909.8149		
929.788	TG 54:0 + K+	-2.9151
905.7888	TG(15:0/22:4(7Z,10Z,13Z,16Z)/O-18:0) + Na	-2.9108
850.8148		
855.7676		
931.8021		
963.842	TG 58:3 + Na+	-2.8567
880.7742	TG(22:6(4Z,7Z,10Z,13Z,16Z,19Z)/14:1(9Z)/O-18:0) + NH4	-2.7696
874.8085		
939.8322	TG 56:1 + Na+	-2.7486
908.8074	TG(16:1(9Z)/22:6(4Z,7Z,10Z,13Z,16Z,19Z)/O-18:0) + NH4	-2.7368
902.8182	TG 54:3 + NH4	-2.7102
853.7538		
964.8472		
903.7783	TG(15:0/22:5(4Z,7Z,10Z,13Z,16Z)/O-18:0) + Na	-2.6083
955.8048	TG(16:0/18:0/22:1(13Z)) + K+	-2.5861
782.5944	PC O-35:1 + Na+	2.5573
848.7873		

Combination vs DMSO

No significant metabolites

Appendix 4: SAM Results for Day 5 Samples in POS Mode

7738 vs DMSO

M/Z values	Lipid	d.value
909.8083		
881.7767		
797.6508	SM(d18:2(4E,14Z)/23:1(9Z)) + H	1.6889
907.7941		
897.7575		
923.7755		
871.7419		
429.2526		
895.7543	TG(15:0/O-18:0/20:3(5Z,8Z,11Z)) + H	-3.4567
898.7701		
925.7857		
921.7628	TG(15:0/22:4(7Z,10Z,13Z,16Z)/O-18:0) + K	-3.25
899.7694		
924.7876		
896.761	TG 54:6 + NH4	-3.0283
872.7512		
947.7762		
869.7442		

922.7727		
945.7669		

Ipilumumab vs DMSO

m/z	Lipid	d.value
766.6001	PG O-35:1 + NH4	10.472
819.5818	PS 37:2 + NH4	6.8223
780.583	PE O-40:5 + H+	6.6057
523.3857	LPC O-18:2 + NH4+	6.4838
893.761	TG 53:3 + Na+	6.448
864.8102	TG 51:1 + NH4+	6.2732
843.7271	SM 44:1;O2 + H+	6.1611
847.7089	PC O-40:0 + NH4+	6.1012
989.8571	TG 60:4 + Na+	5.7318
691.5197	PA 35:0 + H+	5.5606
963.842	TG 58:3 + Na+	5.2918
810.6276	PE O-42:4 + H+	5.1388
846.743	SM 43:1;O2 + NH4+	5.0323
965.8553	TG 58:2 + Na+	4.785
997.7976	TG 58:3 + K+	4.7762
924.7945	TG 56:6 + NH4+	4.5269
939.8322	TG 56:1 + Na+	4.0445
898.7768	TG 54:5 + NH4+	3.7818
719.5926	PA O-38:0 + Na+	-3.768
870.7524	TG 52:5 + NH4+	-4.3494
413.2806	LPC O-10:1 + NH4+	-4.7249

414.2848	NA 24:4;O + K+	-5.4198
913.8103	TG 54:0 + Na+	-6.6015
674.6176	Cer 42:0;O + K+	-6.7837
940.8328	TG 57:5 + NH4+	-7.2325
977.7988	TG 58:4 + K+	-7.2376
955.8048	TG 56:1 + K+	-7.5618
981.8191	TG 58:2 + K+	-7.5818
958.8258	PC 48:0 + H+	-7.8512
693.5467	DG 40:5 + Na+	-7.8657

Nivolumab vs DMSO

M/Z	Lipids	d.value
780.583	PE O-40:5 + H+	6.0298
673.6132		
863.7912		
413.2806	LPC O-10:1 +NH4+	-4.1655
880.7742	TG(14:1(9Z)/22:6(4Z,7Z,10Z,13Z,16Z,19Z)/O-18:0) + NH4+	4.1606
997.7976	TG (16:0/20:1(11z)/22:2	4.1422
849.7485	PC O-40:0 +NH4+	4.0816
903.7783	TG(15:0/22:5(4Z,7Z,10Z,13Z,16Z)/O-18:0) + Na+	4.0345
786.6263		
414.2848	NA 24:4;O + K+	-3.9644
819.5818	PS 37:2 + NH4+	3.6329
827.7368		

829.7519		
867.7668		
853.7538		
979.8094	TG 58:3 + K+	3.4757
847.7089		
876.831		
523.3857	LPC O-18:2 +NH4+	3.4015
893.761	TG 53:3 +Na+	3.3404
691.5197	PA 35:0	3.2851
950.8066		
856.7731	TG(14:1(9Z)/20:4(5Z,8Z,11Z,14Z)/O-18:0 + NH4	-3.2144
429.2559		
865.7679	TG(14:1(9Z)/22:5(4Z,7Z,10Z,13Z,16Z)/O-18:0) + H+	3.2042
854.7585	TG(14:1(9Z)/20:5(5Z,8Z,11Z,14Z,17Z)/O-18:0) + NH4+	-3.1383
808.5929	PC 38:5	3.0891
671.5959		
815.6829		
864.8102	TG 51:1	3.0219
811.6498		
963.842	TG 58:3	2.82
872.7574		
870.7524	TG 52:5	-2.7557
884.8179		
877.8083		
877.7585	TG(15:0/O-18:0/20:4(8Z,11Z,	-2.7174

	14Z,17Z)) + Na+	
883.8054	TG(15:0/20:1(11Z)/O-18:0) + Na+	2.7009
954.8099		
938.8493	TG(18:0/22:6(4Z,7Z,10Z,13Z,16Z,19Z)/O-18:0) + NH4+	2.5847
804.5776	PS(18:1(9Z)/19:0) + H+	-2.5258
965.8553	TG 58:2	2.523
674.6176	Cer 42:0;O	-2.5144
855.7676		
955.8048	TG 56:1	-2.5008
904.7943		
843.7271	SM 44:1;O2	2.4591
851.7522		
928.7964		
828.7411	TG(14:1(9Z)/O-18:0/18:4(6Z,9Z,12Z,15Z)) + NH4+	-2.4517
956.815		
958.8258	PC 48:0	-2.4375
858.7834		
981.8191	TG 58:2	-2.4116

Nivolumab + Ipilimumab vs DMSO

M/Z Value	Lipid	d.value
673.6132		
780.583	PE O-40:5 + H+	3.9791
413.2806	LPC O-10:1 + NH4+	-3.6223
414.2848	NA 24:4;O + K+	-3.2157

863.7912		
853.7538		
856.7731	TG(14:1(9Z)/20:4(5Z,8Z,11Z,14Z)/O-1 + NH4+	-2.9009
997.7976		
827.7368		
867.7668		
829.7519		
849.7485	PC O-40:0 + NH4+	2.7923
786.6263		
854.7585	TG(14:1(9Z)/20:5(5Z,8Z,11Z,14Z,17Z)/O-18:0) + NH4+	-2.7191
876.831		
429.2559		
671.5959		
880.7742	TG(14:1(9Z)/22:6(4Z,7Z,10Z,13Z,16Z,19Z)/O-18:0) + NH4+	2.4538
847.7089		
877.7585	TG(15:0/O-18:0/20:4(8Z,11Z,14Z,17Z)) + Na+	-2.3818
691.5197	PA 35:0 + H+	2.3753
819.5818	PS 37:2 + NH4+	2.3575
523.3857	LPC O-18:2 + NH4+	2.3542
877.8083		
950.8066		
903.7783	TG(15:0/22:5(4Z,7Z,10Z,13Z,16Z)/O-18:0) + Na+	2.2377
872.7574		

870.7524	TG 52:5 + NH4+	-2.2118
808.5929	PC 38:5 + H+	2.2046
979.8094	TG 58:3 + K+	2.189
893.761	TG 53:3 + Na+	2.1846
955.8048	TG 56:1 + K+	-2.1801
815.6829		
864.8102	TG 51:1 + NH4+	2.1129
851.7522		
811.6498		
828.7411	TG(14:1(9Z)/O-18:0/18:4(6Z,9Z,12Z,15Z)) + NH4+	-2.0788
865.7679	TG(14:1(9Z)/22:5(4Z,7Z,10Z,13Z,16Z)/O-18:0) + H	2.0764
954.8099		
804.5776	PS(18:1(9Z)/19:0) + H+	-2.0676
674.6176	Cer 42:0;O + K+	-2.0645
882.7889	TG(14:1(9Z)/22:5(4Z,7Z,10Z,13Z,16Z)/O-18:0) + NH4+	-1.9998
901.7731		
874.8085		
958.8258	PC 48:0 + H+	-1.9654
963.842	TG 58:3 + Na+	1.958
367.258		
981.8191	TG 58:2 + K+	-1.9043
858.7834		
919.7549	TG(15:0/22:5(4Z,7Z,10Z,13Z,16Z)/O-18:0) + K+	-1.8487
913.8103	TG 54:0 + Na+	-1.8266

695.5944		
841.7466		
908.8074	TG(16:1(9Z)/22:6(4Z,7Z,10Z,13Z,16Z,19Z)/O-18:0) + NH4+	-1.79
956.815		
766.6001	PG O-35:1 + NH4+	1.7471
977.7988	TG 58:4 + K+	-1.6837
803.5738	PG 38:2 + H+	-1.6181
825.7199		

Stimulated Immune Cells vs DMSO

M/Z		d.value
780.583	PE O-40:5 + H+	2.3297
413.2806	LPC O-10:1 NH4+	-2.266
880.7742	TG(14:1(9Z)/22:6(4Z,7Z,10Z,13Z,16Z,19Z)/O-18:0) + NH4	2.1755
673.6132		
997.7976		
853.7538		
414.2848	NA 24:4;O + K+	-1.73
863.7912		
849.7485	PC O-40:0 NH4+	1.615
429.2559		
903.7783	TG(15:0/22:5(4Z,7Z,10Z,13Z,16Z)/O-18:0 + Na+	1.5596
979.8094	TG 58:3 + K+	1.4911
786.6263		

NUC-7738 + Nivolumab vs DMSO

No significant Metabolites

Combination vs DMSO

No significant Metabolites